

## An improved search for the electric dipole moment of the $\tau$ lepton

K. Inami,<sup>53</sup> K. Hayasaka,<sup>61</sup> I. Adachi,<sup>16,12</sup> H. Aihara,<sup>85</sup> S. Al Said,<sup>78,36</sup> D. M. Asner,<sup>3</sup> V. Aulchenko,<sup>4,62</sup> T. Aushev,<sup>18</sup> R. Ayad,<sup>78</sup> V. Babu,<sup>8</sup> S. Bahinipati,<sup>21</sup> P. Behera,<sup>24</sup> M. Bessner,<sup>15</sup> B. Bhuyan,<sup>22</sup> T. Bilka,<sup>5</sup> J. Biswal,<sup>32</sup> A. Bobrov,<sup>4,62</sup> G. Bonvicini,<sup>89</sup> A. Bozek,<sup>59</sup> M. Bračko,<sup>92</sup> T. E. Browder,<sup>15</sup> M. Campajola,<sup>29,55</sup> D. Červenkov,<sup>5</sup> B. G. Cheon,<sup>14</sup> K. Chilikin,<sup>42</sup> H. E. Cho,<sup>14</sup> K. Cho,<sup>38</sup> Y. Choi,<sup>76</sup> S. Choudhury,<sup>23</sup> D. Cinabro,<sup>89</sup> S. Cunliffe,<sup>8</sup> S. Das,<sup>46</sup> G. De Nardo,<sup>29,55</sup> R. Dhamija,<sup>23</sup> F. Di Capua,<sup>29,55</sup> Z. Doležal,<sup>5</sup> T. V. Dong,<sup>10</sup> S. Dubey,<sup>15</sup> S. Eidelman,<sup>4,62,42</sup> D. Epifanov,<sup>4,62</sup> T. Ferber,<sup>8</sup> B. G. Fulsom,<sup>64</sup> R. Garg,<sup>65</sup> V. Gaur,<sup>88</sup> N. Gabyshev,<sup>4,62</sup> A. Garmash,<sup>4,62</sup> A. Giri,<sup>23</sup> P. Goldenzweig,<sup>33</sup> B. Golob,<sup>44,32</sup> D. Greenwald,<sup>80</sup> K. Gudkova,<sup>4,62</sup> C. Hadjivasiliou,<sup>64</sup> O. Hartbrich,<sup>15</sup> H. Hayashii,<sup>56</sup> M. T. Hedges,<sup>15</sup> W.-S. Hou,<sup>58</sup> C.-L. Hsu,<sup>77</sup> T. Iijima,<sup>54,53</sup> G. Inguglia,<sup>27</sup> A. Ishikawa,<sup>16,12</sup> R. Itoh,<sup>16,12</sup> M. Iwasaki,<sup>63</sup> Y. Iwasaki,<sup>16</sup> W. W. Jacobs,<sup>25</sup> E.-J. Jang,<sup>13</sup> Y. Jin,<sup>85</sup> C. W. Joo,<sup>34</sup> K. K. Joo,<sup>6</sup> Y. Kato,<sup>53</sup> T. Kawasaki,<sup>37</sup> H. Kichimi,<sup>16</sup> C. Kiesling,<sup>48</sup> C. H. Kim,<sup>14</sup> D. Y. Kim,<sup>75</sup> S. H. Kim,<sup>72</sup> Y.-K. Kim,<sup>91</sup> T. D. Kimmel,<sup>88</sup> K. Kinoshita,<sup>7</sup> P. Kodyš,<sup>5</sup> T. Konno,<sup>37</sup> S. Korpar,<sup>92</sup> P. Križan,<sup>44,32</sup> R. Kroeger,<sup>50</sup> P. Krokovny,<sup>4,62</sup> R. Kulasiri,<sup>35</sup> M. Kumar,<sup>46</sup> R. Kumar,<sup>68</sup> K. Kumara,<sup>89</sup> Y.-J. Kwon,<sup>91</sup> K. Lalwani,<sup>46</sup> J. S. Lange,<sup>11</sup> S. C. Lee,<sup>40</sup> C. H. Li,<sup>43</sup> J. Li,<sup>40</sup> L. K. Li,<sup>7</sup> Y. B. Li,<sup>66</sup> L. Li Gioi,<sup>48</sup> J. Libby,<sup>24</sup> D. Liventsev,<sup>89,16</sup> C. MacQueen,<sup>49</sup> M. Masuda,<sup>84,69</sup> T. Matsuda,<sup>51</sup> D. Matvienko,<sup>4,62,42</sup> M. Merola,<sup>29,55</sup> F. Metzner,<sup>33</sup> K. Miyabayashi,<sup>56</sup> R. Mizuk,<sup>42,18</sup> G. B. Mohanty,<sup>79</sup> S. Mohanty,<sup>79,87</sup> T. J. Moon,<sup>72</sup> M. Nakao,<sup>16,12</sup> A. Natochii,<sup>15</sup> L. Nayak,<sup>23</sup> M. Nayak,<sup>81</sup> N. K. Nisar,<sup>3</sup> S. Nishida,<sup>16,12</sup> S. Ogawa,<sup>82</sup> H. Ono,<sup>60,61</sup> Y. Onuki,<sup>85</sup> P. Oskin,<sup>42</sup> P. Pakhlov,<sup>42,52</sup> G. Pakhlova,<sup>18,42</sup> S. Pardi,<sup>29</sup> S.-H. Park,<sup>91</sup> S. Paul,<sup>80,48</sup> T. K. Pedlar,<sup>45</sup> R. Pestotnik,<sup>32</sup> L. E. Piilonen,<sup>88</sup> T. Podobnik,<sup>44,32</sup> V. Popov,<sup>18</sup> E. Prencipe,<sup>19</sup> M. T. Prim,<sup>33</sup> A. Rabusov,<sup>80</sup> M. Röhrken,<sup>8</sup> A. Rostomyan,<sup>8</sup> N. Rout,<sup>24</sup> G. Russo,<sup>55</sup> D. Sahoo,<sup>79</sup> S. Sandilya,<sup>23</sup> A. Sangal,<sup>7</sup> L. Santelj,<sup>44,32</sup> T. Sanuki,<sup>83</sup> V. Savinov,<sup>67</sup> G. Schnell,<sup>1,20</sup> C. Schwanda,<sup>27</sup> Y. Seino,<sup>61</sup> K. Senyo,<sup>90</sup> M. E. Sevier,<sup>49</sup> M. Shapkin,<sup>28</sup> C. Sharma,<sup>46</sup> J.-G. Shiu,<sup>58</sup> B. Shwartz,<sup>4,62</sup> F. Simon,<sup>48</sup> E. Solovieva,<sup>42</sup> M. Starič,<sup>32</sup> Z. S. Stottler,<sup>88</sup> J. F. Strube,<sup>64</sup> K. Sumisawa,<sup>16,12</sup> W. Sutcliffe,<sup>2</sup> M. Takizawa,<sup>73,17,70</sup> U. Tamponi,<sup>30</sup> K. Tanida,<sup>31</sup> Y. Tao,<sup>9</sup> F. Tenchini,<sup>8</sup> K. Trabelsi,<sup>41</sup> M. Uchida,<sup>86</sup> S. Uehara,<sup>16,12</sup> S. Uno,<sup>16,12</sup> Y. Ushiroda,<sup>16,12</sup> R. Van Tonder,<sup>2</sup> G. Varner,<sup>15</sup> A. Vinokurova,<sup>4,62</sup> C. H. Wang,<sup>57</sup> E. Wang,<sup>67</sup> P. Wang,<sup>26</sup> M. Watanabe,<sup>61</sup> S. Watanuki,<sup>41</sup> E. Won,<sup>39</sup> X. Xu,<sup>74</sup> B. D. Yabsley,<sup>77</sup> W. Yan,<sup>71</sup> S. B. Yang,<sup>39</sup> H. Ye,<sup>8</sup> J. H. Yin,<sup>39</sup> Y. Yusa,<sup>61</sup> Z. P. Zhang,<sup>71</sup> V. Zhilich,<sup>4,62</sup> and V. Zhukova<sup>42</sup>

(The Belle Collaboration)

<sup>1</sup>University of the Basque Country UPV/EHU, 48080 Bilbao

<sup>2</sup>University of Bonn, 53115 Bonn

<sup>3</sup>Brookhaven National Laboratory, Upton, New York 11973

<sup>4</sup>Budker Institute of Nuclear Physics SB RAS, Novosibirsk 630090

<sup>5</sup>Faculty of Mathematics and Physics, Charles University, 121 16 Prague

<sup>6</sup>Chonnam National University, Gwangju 61186

<sup>7</sup>University of Cincinnati, Cincinnati, Ohio 45221

<sup>8</sup>Deutsches Elektronen-Synchrotron, 22607 Hamburg

<sup>9</sup>University of Florida, Gainesville, Florida 32611

<sup>10</sup>Key Laboratory of Nuclear Physics and Ion-beam Application (MOE)

and Institute of Modern Physics, Fudan University, Shanghai 200443

<sup>11</sup>Justus-Liebig-Universität Gießen, 35392 Gießen

<sup>12</sup>SOKENDAI (The Graduate University for Advanced Studies), Hayama 240-0193

<sup>13</sup>Gyeongsang National University, Jinju 52828

<sup>14</sup>Department of Physics and Institute of Natural Sciences, Hanyang University, Seoul 04763

<sup>15</sup>University of Hawaii, Honolulu, Hawaii 96822

<sup>16</sup>High Energy Accelerator Research Organization (KEK), Tsukuba 305-0801

<sup>17</sup>J-PARC Branch, KEK Theory Center, High Energy Accelerator Research Organization (KEK), Tsukuba 305-0801

<sup>18</sup>Higher School of Economics (HSE), Moscow 101000

<sup>19</sup>Forschungszentrum Jülich, 52425 Jülich

<sup>20</sup>IKERBASQUE, Basque Foundation for Science, 48013 Bilbao

<sup>21</sup>Indian Institute of Technology Bhubaneswar, Satya Nagar 751007

<sup>22</sup>Indian Institute of Technology Guwahati, Assam 781039

<sup>23</sup>Indian Institute of Technology Hyderabad, Telangana 502285

<sup>24</sup>Indian Institute of Technology Madras, Chennai 600036

- <sup>25</sup>Indiana University, Bloomington, Indiana 47408
- <sup>26</sup>Institute of High Energy Physics, Chinese Academy of Sciences, Beijing 100049
- <sup>27</sup>Institute of High Energy Physics, Vienna 1050
- <sup>28</sup>Institute for High Energy Physics, Protvino 142281
- <sup>29</sup>INFN - Sezione di Napoli, 80126 Napoli
- <sup>30</sup>INFN - Sezione di Torino, 10125 Torino
- <sup>31</sup>Advanced Science Research Center, Japan Atomic Energy Agency, Naka 319-1195
- <sup>32</sup>J. Stefan Institute, 1000 Ljubljana
- <sup>33</sup>Institut für Experimentelle Teilchenphysik, Karlsruher Institut für Technologie, 76131 Karlsruhe
- <sup>34</sup>Kavli Institute for the Physics and Mathematics of the Universe (WPI), University of Tokyo, Kashiwa 277-8583
- <sup>35</sup>Kennesaw State University, Kennesaw, Georgia 30144
- <sup>36</sup>Department of Physics, Faculty of Science, King Abdulaziz University, Jeddah 21589
- <sup>37</sup>Kitasato University, Sagamihara 252-0373
- <sup>38</sup>Korea Institute of Science and Technology Information, Daejeon 34141
- <sup>39</sup>Korea University, Seoul 02841
- <sup>40</sup>Kyungpook National University, Daegu 41566
- <sup>41</sup>Université Paris-Saclay, CNRS/IN2P3, IJCLab, 91405 Orsay
- <sup>42</sup>P.N. Lebedev Physical Institute of the Russian Academy of Sciences, Moscow 119991
- <sup>43</sup>Liaoning Normal University, Dalian 116029
- <sup>44</sup>Faculty of Mathematics and Physics, University of Ljubljana, 1000 Ljubljana
- <sup>45</sup>Luther College, Decorah, Iowa 52101
- <sup>46</sup>Malaviya National Institute of Technology Jaipur, Jaipur 302017
- <sup>47</sup>University of Maribor, 2000 Maribor
- <sup>48</sup>Max-Planck-Institut für Physik, 80805 München
- <sup>49</sup>School of Physics, University of Melbourne, Victoria 3010
- <sup>50</sup>University of Mississippi, University, Mississippi 38677
- <sup>51</sup>University of Miyazaki, Miyazaki 889-2192
- <sup>52</sup>Moscow Physical Engineering Institute, Moscow 115409
- <sup>53</sup>Graduate School of Science, Nagoya University, Nagoya 464-8602
- <sup>54</sup>Kobayashi-Maskawa Institute, Nagoya University, Nagoya 464-8602
- <sup>55</sup>Università di Napoli Federico II, 80126 Napoli
- <sup>56</sup>Nara Women's University, Nara 630-8506
- <sup>57</sup>National United University, Miao Li 36003
- <sup>58</sup>Department of Physics, National Taiwan University, Taipei 10617
- <sup>59</sup>H. Niewodniczanski Institute of Nuclear Physics, Krakow 31-342
- <sup>60</sup>Nippon Dental University, Niigata 951-8580
- <sup>61</sup>Niigata University, Niigata 950-2181
- <sup>62</sup>Novosibirsk State University, Novosibirsk 630090
- <sup>63</sup>Osaka City University, Osaka 558-8585
- <sup>64</sup>Pacific Northwest National Laboratory, Richland, Washington 99352
- <sup>65</sup>Punjab University, Chandigarh 160014
- <sup>66</sup>Peking University, Beijing 100871
- <sup>67</sup>University of Pittsburgh, Pittsburgh, Pennsylvania 15260
- <sup>68</sup>Punjab Agricultural University, Ludhiana 141004
- <sup>69</sup>Research Center for Nuclear Physics, Osaka University, Osaka 567-0047
- <sup>70</sup>Meson Science Laboratory, Cluster for Pioneering Research, RIKEN, Saitama 351-0198
- <sup>71</sup>Department of Modern Physics and State Key Laboratory of Particle Detection and Electronics, University of Science and Technology of China, Hefei 230026
- <sup>72</sup>Seoul National University, Seoul 08826
- <sup>73</sup>Showa Pharmaceutical University, Tokyo 194-8543
- <sup>74</sup>Soochow University, Suzhou 215006
- <sup>75</sup>Soongsil University, Seoul 06978
- <sup>76</sup>Sungkyunkwan University, Suwon 16419
- <sup>77</sup>School of Physics, University of Sydney, New South Wales 2006
- <sup>78</sup>Department of Physics, Faculty of Science, University of Tabuk, Tabuk 71451
- <sup>79</sup>Tata Institute of Fundamental Research, Mumbai 400005
- <sup>80</sup>Department of Physics, Technische Universität München, 85748 Garching
- <sup>81</sup>School of Physics and Astronomy, Tel Aviv University, Tel Aviv 69978
- <sup>82</sup>Toho University, Funabashi 274-8510
- <sup>83</sup>Department of Physics, Tohoku University, Sendai 980-8578
- <sup>84</sup>Earthquake Research Institute, University of Tokyo, Tokyo 113-0032
- <sup>85</sup>Department of Physics, University of Tokyo, Tokyo 113-0033
- <sup>86</sup>Tokyo Institute of Technology, Tokyo 152-8550
- <sup>87</sup>Utkal University, Bhubaneswar 751004

<sup>88</sup>Virginia Polytechnic Institute and State University, Blacksburg, Virginia 24061

<sup>89</sup>Wayne State University, Detroit, Michigan 48202

<sup>90</sup>Yamagata University, Yamagata 990-8560

<sup>91</sup>Yonsei University, Seoul 03722

<sup>92</sup>Faculty of Chemistry and Chemical Engineering, University of Maribor, 2000 Maribor, Slovenia

We report a measurement of the electric dipole moment of the  $\tau$  lepton ( $d_\tau$ ) using an  $833 \text{ fb}^{-1}$  data sample collected near the  $\Upsilon(4S)$  resonance, with the Belle detector at the KEKB asymmetric-energy  $e^+e^-$  collider. Using an optimal observable method, we obtain the real and imaginary parts of  $d_\tau$  as  $\text{Re}(d_\tau) = (-0.62 \pm 0.63) \times 10^{-17} \text{ ecm}$  and  $\text{Im}(d_\tau) = (-0.40 \pm 0.32) \times 10^{-17} \text{ ecm}$ , respectively. These results are consistent with no electric dipole moment at the present level of experimental sensitivity and improve the sensitivity by about a factor of three.

PACS numbers: 13.40.Gp, 13.35.Dx, 14.60.Fg

The electric dipole moment (EDM) of the  $\tau$  lepton is a fundamental parameter that parameterizes time-reversal ( $T$ ) or charge-conjugation–parity ( $CP$ ) violation at the  $\gamma\tau\tau$  vertex. In the Standard Model (SM),  $CP$  violation arises due to an irreducible phase in the CKM matrix [1], which predicts an unobservably small  $\tau$ -lepton EDM ( $d_\tau$ ) of order  $10^{-37} \text{ ecm}$  [2]. Hence, observation of a nonzero  $d_\tau$  value would be a clear sign of new physics. Some new physics models indicate a larger EDM of order  $10^{-19} \text{ ecm}$  [3].

The most sensitive previous measurement set an upper limit on the EDM of order  $10^{-17} \text{ ecm}$  [4]; the results were obtained by the Belle collaboration [5] using  $29.5 \text{ fb}^{-1}$  of data collected at the KEKB collider [6] at the center-of-mass (CM) energy  $\sqrt{s} = 10.58 \text{ GeV}$ . The obtained real and imaginary parts of  $d_\tau$  were  $\text{Re}(d_\tau) = (1.15 \pm 1.70) \times 10^{-17} \text{ ecm}$  and  $\text{Im}(d_\tau) = (-0.83 \pm 0.86) \times 10^{-17} \text{ ecm}$ , respectively, and the corresponding limits were  $-2.2 \times 10^{-17} < \text{Re}(d_\tau) < 4.5 \times 10^{-17} \text{ ecm}$  and  $-2.5 \times 10^{-17} < \text{Im}(d_\tau) < 0.8 \times 10^{-17} \text{ ecm}$ .

In this paper, we present updated results on  $d_\tau$  using a much larger sample of  $833 \text{ fb}^{-1}$  Belle data:  $571 \text{ fb}^{-1}$  collected at the  $\Upsilon(4S)$  resonance,  $74 \text{ fb}^{-1}$  collected  $60 \text{ MeV}$  below it, and  $188 \text{ fb}^{-1}$  collected near the  $\Upsilon(1S)$ ,  $\Upsilon(2S)$ ,  $\Upsilon(3S)$ , and  $\Upsilon(5S)$  resonances. The data samples are independent from the one used in the previous Belle result. The sensitivity for  $\text{Re}(d_\tau)$  and  $\text{Im}(d_\tau)$  has improved by about a factor of three, due to the increase of the data statistics.

The effective Lagrangian for  $\tau$ -pair production including the EDM term in the vertex is

$$\mathcal{L} = \bar{\tau}[-eQ\gamma^\mu A_\mu - id_\tau\sigma^{\mu\nu}\gamma_5\partial_\mu A_\nu]\tau. \quad (1)$$

Including the EDM term, the squared spin-density matrix ( $\chi_{\text{prod}}$ ) for the production vertex in the process  $e^+e^- \rightarrow \tau^+\tau^-$  is given by [7]

$$\chi_{\text{prod}} = \chi_{\text{SM}} + \text{Re}(d_\tau)\chi_{\text{Re}} + \text{Im}(d_\tau)\chi_{\text{Im}} + |d_\tau|^2\chi_{d^2}, \quad (2)$$

where  $\chi_{\text{SM}}$  is the SM term, and  $\chi_{\text{Re}}$  and  $\chi_{\text{Im}}$  are the interference terms between the SM and the EDM for the real and imaginary parts of  $d_\tau$ . Here,  $\chi_{d^2}$  is a higher-order

EDM term, which we can neglect since  $d_\tau$  is small. The matrix elements in Eq. (2) can be expressed using the momenta of the electron beam and the  $\tau$  lepton, and the spins of  $\tau^+$  and  $\tau^-$  in the  $e^+e^-$  CM frame. The interference terms are proportional to  $CP$ -odd spin-momentum correlation terms

$$\chi_{\text{Re}} \propto -\{m_\tau + (k_0 - m_\tau)(\hat{\mathbf{k}} \cdot \hat{\mathbf{p}})^2\}(\mathbf{S}_+ \times \mathbf{S}_-) \cdot \hat{\mathbf{k}} + k_0(\hat{\mathbf{k}} \cdot \hat{\mathbf{p}})(\mathbf{S}_+ \times \mathbf{S}_-) \cdot \hat{\mathbf{p}}, \quad (3)$$

$$\chi_{\text{Im}} \propto -\{m_\tau + (k_0 - m_\tau)(\hat{\mathbf{k}} \cdot \hat{\mathbf{p}})^2\}(\mathbf{S}_+ - \mathbf{S}_-) \cdot \hat{\mathbf{k}} + k_0(\hat{\mathbf{k}} \cdot \hat{\mathbf{p}})(\mathbf{S}_+ - \mathbf{S}_-) \cdot \hat{\mathbf{p}}, \quad (4)$$

where  $k_0$  is the energy of the  $\tau^\pm$ ,  $m_\tau$  is the  $\tau$  mass,  $\mathbf{p}$  is the three-momentum of the  $e^+$ ,  $\mathbf{k}$  is the three-momentum of the  $\tau^+$ ,  $\mathbf{S}_\pm$  are the spin vectors for the  $\tau^\pm$ , and hats denote unit momenta. In Eqs. (3) and (4) above,  $\chi_{\text{Re}}$  is  $T$ -odd and  $\chi_{\text{Im}}$  is  $T$ -even. A more detailed discussion is given in Ref. [4].

Several  $CP$ -violating observables have been proposed in the literature [3]. For this analysis, we use the so-called optimal observable method [8] to obtain the  $d_\tau$  values. The optimal observables are

$$\mathcal{O}_{\text{Re}} = \frac{\chi_{\text{Re}}}{\chi_{\text{SM}}}, \quad \mathcal{O}_{\text{Im}} = \frac{\chi_{\text{Im}}}{\chi_{\text{SM}}}. \quad (5)$$

They maximize sensitivity to the  $\tau$  EDM. The mean values of these observables ( $\langle \mathcal{O}_{\text{Re}} \rangle$ ,  $\langle \mathcal{O}_{\text{Im}} \rangle$ ) are linearly dependent on  $\text{Re}(d_\tau)$  and  $\text{Im}(d_\tau)$ ,

$$\langle \mathcal{O}_{\text{Re}} \rangle = a_{\text{Re}}\text{Re}(d_\tau) + b_{\text{Re}}, \quad \langle \mathcal{O}_{\text{Im}} \rangle = a_{\text{Im}}\text{Im}(d_\tau) + b_{\text{Im}}, \quad (6)$$

since

$$\begin{aligned} \langle \mathcal{O}_{\text{Re}} \rangle &\propto \int \mathcal{O}_{\text{Re}}\chi_{\text{prod}}d\phi \\ &= \int \chi_{\text{Re}}d\phi + \text{Re}(d_\tau) \int \frac{(\chi_{\text{Re}})^2}{\chi_{\text{SM}}}d\phi, \end{aligned} \quad (7)$$

where the integration is performed over the available phase space  $\phi$  and

$$a_{\text{Re}} = \int \frac{(\chi_{\text{Re}})^2}{\chi_{\text{SM}}}d\phi, \quad b_{\text{Re}} = \int \chi_{\text{Re}}d\phi. \quad (8)$$

The expression for  $\mathcal{O}_{\text{Im}}$  is identical with the exchange of “Re” and “Im” in Eqs. (7) and (8). The cross-term containing the integral of the product of  $\chi_{\text{Re}}$  and  $\chi_{\text{Im}}$  drops out because of their different symmetry properties. To determine the coefficients, we have performed the integration using Monte Carlo (MC) samples in order to account for detector effects. In principle, the constant term ( $b_{\text{Re/Im}}$ ) should be zero as  $\chi_{\text{Re/Im}}$  is symmetric, but can be nonzero owing to nonuniform acceptance of the detector. We therefore add this term. Using linear relations,  $\text{Re}(d_\tau)$  and  $\text{Im}(d_\tau)$  can be obtained from the measured values of  $\langle \mathcal{O}_{\text{Re/Im}} \rangle$ .

We have used the data collected by the Belle detector for this analysis. Belle is a large-solid-angle magnetic spectrometer that consists of a silicon vertex detector, a 50-layer central drift chamber (CDC), an array of aerogel threshold Cherenkov counters (ACC), a barrel-like arrangement of time-of-flight scintillation counters (TOF), and an electromagnetic calorimeter (ECL) comprised of CsI(Tl) crystals; all located inside a superconducting solenoid coil that provides a 1.5 T magnetic field. An iron flux-return yoke located outside of the coil is instrumented to detect  $K_L^0$  mesons and muons (KLM). The detector is described in detail elsewhere [5].

The MC event generators KKMC and TAUOLA [9] are used for  $\tau$ -pair production and decays, respectively. Detector simulation is performed by a GEANT3 [10] based program. We use a sample of MC events corresponding to about five times the data luminosity. In order to study the background contamination arising from non  $\tau$ -pair events, we generate MC samples for the  $e^+e^- \rightarrow q\bar{q}$  ( $q = u, d, c, s$ ) continuum and  $e^+e^- \rightarrow \Upsilon(4S) \rightarrow B\bar{B}$  events using the EVTGEN [11] program, and for two-photon mediated processes ( $e^+e^- \rightarrow e^+e^-\ell^+\ell^-$ ,  $e^+e^-q\bar{q}$ ) using the AAFH [12] program.

We use  $\tau$ -pair events with a 1-prong versus 1-prong topology in which the particles are selected by the following criteria. Charged tracks are required to have a transverse momentum of  $p_T > 0.1$  GeV/ $c$  and an impact parameter along the positron beam and in the transverse plane less than 3.0 cm and 1.0 cm, respectively. An ECL cluster not matching any track is identified as a photon candidate. Photon candidates should deposit an energy of  $E > 0.1$  GeV in the ECL. Each charged particle is identified using a likelihood ratio formed combining the ionization energy loss in the CDC, the ratio of energy deposited in the ECL and momentum measured in the CDC, the shower shape in the ECL, the position matching of the ECL cluster and CDC track, the range and hit pattern in the KLM, the time-of-flight information from the TOF, and the light yield of the ACC. Electron and muon candidates are selected by requiring the likelihood ratios  $\mathcal{P}(e)$  [13] and  $\mathcal{P}(\mu)$  [14] to exceed 0.9 and 0.95, respectively. The corresponding identification efficiency is above 90% with a pion misidentification rate less than 2%. Charged pions and kaons are distinguished using

likelihood ratios,  $\mathcal{P}(i/j) = \mathcal{L}_i/(\mathcal{L}_i + \mathcal{L}_j)$ , where  $\mathcal{L}_i$  is the likelihood for a track to be identified as  $i$ . Pion candidates for the  $\tau \rightarrow \pi\nu$  mode are selected by requiring  $\mathcal{P}(K/\pi) < 0.8$ ,  $\mathcal{P}(\mu) < 0.05$ ,  $\mathcal{P}(e) < 0.01$ , and an electron likelihood ratio obtained by combining information from the ACC and CDC less than 0.9 to reduce electron backgrounds, which do not interact in the ECL. The requirement  $\mathcal{P}(K/\pi) < 0.8$  rejects 78% of kaons, while 94% of muons are rejected by the requirement  $\mathcal{P}(\mu) < 0.05$  and 98% of electrons are rejected by the requirement  $\mathcal{P}(e) < 0.01$ . A  $\rho^\pm$  is reconstructed from a charged track and a  $\pi^0$ , requiring the opening angle between them to be less than  $90^\circ$  in the CM frame and the charged track not to be an electron or a muon. The  $\rho^\pm$  candidates include higher  $\rho$  resonances since no mass cut is applied. The  $\pi^0$  candidates, reconstructed from  $\gamma\gamma$  combinations, should have an invariant mass between 110 and 150 MeV/ $c^2$  and a momentum of  $p > 0.2$  GeV/ $c$ .

We select eight exclusive final states of the  $\tau$ -pair process  $\tau\tau \rightarrow (e\nu)(\mu\nu)$ ,  $(e\nu)(\pi\nu)$ ,  $(\mu\nu)(\pi\nu)$ ,  $(e\nu)(\rho\nu)$ ,  $(\mu\nu)(\rho\nu)$ ,  $(\pi\nu)(\rho\nu)$ ,  $(\rho\nu)(\rho\nu)$ , and  $(\pi\nu)(\pi\nu)$ . Hereafter, we express these final states as  $e\mu$ ,  $e\pi$ ,  $\mu\pi$ ,  $e\rho$ ,  $\mu\rho$ ,  $\pi\rho$ ,  $\rho\rho$ , and  $\pi\pi$ , respectively. We require two charged tracks with zero net charge and no photons except for the daughters of the  $\rho^\pm$  in each event. The sum of the momenta of charged tracks and photons should be less than 9 GeV/ $c$ . (All kinematical values are defined in the laboratory frame, unless otherwise noted.) In order to reduce the background and enhance the particle-identification separation power, the lepton is required to be within the barrel region,  $-0.60 < \cos\theta < 0.83$ , while the  $\pi^\pm$  is required to be within  $-0.50 < \cos\theta < 0.62$ , where  $\cos\theta$  is the cosine of the polar angle. Furthermore, we require the momentum to be greater than 0.5 GeV/ $c$  for an electron, 1.2 GeV/ $c$  for a muon or pion, and 1.0 GeV/ $c$  for a  $\rho^\pm$ .

In order to suppress two-photon mediated background contributions, we require the missing momentum vector not to point along the beam pipe,  $-0.950 < \cos\theta_{\text{missing}} < 0.985$ . To reject Bhabha scattering and  $\mu\mu$  backgrounds, we require the sum of the charged track momenta in the CM frame be less than 9.0 GeV/ $c$ . For the  $e\pi$  mode, we remove events if at least one of the following conditions is satisfied: the opening angle between the two charged particles in the plane perpendicular to the beam axis is greater than  $175^\circ$ , the sum of the charged track momenta in the CM frame is greater than 6.0 GeV/ $c$ , or the  $E_{\text{ECL}}/p$  of pion is larger than 1.05. These criteria are required because of the large contamination from radiative Bhabha events. In addition, for the  $e\rho$  mode, we require that the electron momentum in the CM frame be less than 5 GeV/ $c$  to suppress the same background.

These selection criteria are similar to those required in the previous analysis, with some changes following updates to the reconstruction software, and updated detector calibration.

To maintain consistency between the data and simulation, the effect of the trigger [15] should be taken into account. A hardware trigger simulator is used for MC samples. We also reject events in which the  $\tau$  flight direction cannot be kinematically reconstructed in the observable calculation discussed below.

The obtained signal yield, purity, and dominant background are listed in Table I. The purity and the background are estimated by MC samples. In some modes,  $\tau$  decays with additional  $\pi^0$  mesons contribute a significant background due to low energy photons that escape detection.

The momentum and  $\cos\theta$  distributions for the obtained samples are shown in Figs. 1 and 2.

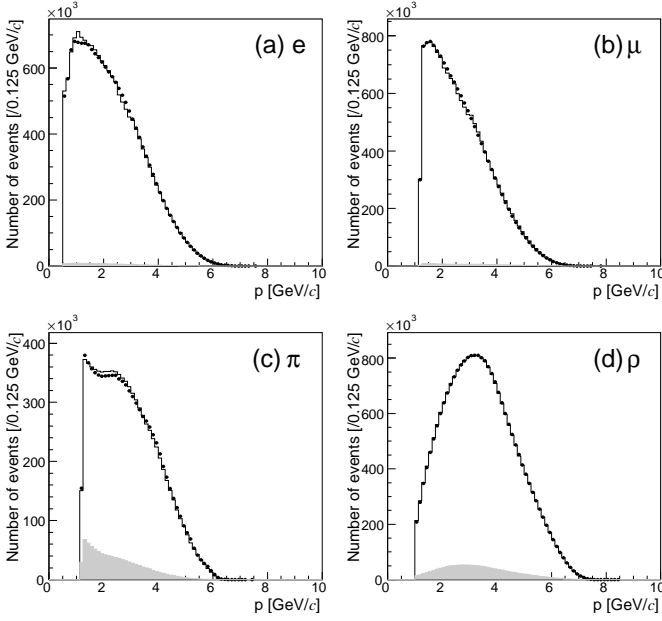


FIG. 1: Momentum distributions of (a) electrons, (b) muons, (c) pions and (d)  $\rho$ 's for the samples obtained after all event selections in each mode. The points with error bars are the data, the histograms are the MC expectation, and the gray shaded histograms are the contribution from misidentification for each particle species.

In order to calculate the observables, we need to determine the  $\tau$  spin vectors and flight direction. The quantities used in the following calculation are obtained in the CM frame. The spin vectors, which give the most probable direction of the spin, are reconstructed using the momenta of  $\tau$  and its decay products [16, 17]. For example, the spin vectors for  $\tau^\pm \rightarrow \pi^\pm \nu_\tau$  are given by

$$\mathbf{S}_\pm = \frac{2}{m_\tau^2 - m_\pi^2} \left( \mp m_\tau \mathbf{p}_{\pi^\pm} + \frac{m_\tau^2 + m_\pi^2 + 2m_\tau E_{\pi^\pm}}{2(E_\tau + m_\tau)} \mathbf{k} \right), \quad (9)$$

where  $\mathbf{p}_{\pi^\pm}$  and  $E_{\pi^\pm}$  are the  $\pi^\pm$  momentum and energy, respectively. (See the Appendix for other decays.) Although the  $\tau$  flight direction  $\hat{\mathbf{k}}$  is necessary to calculate

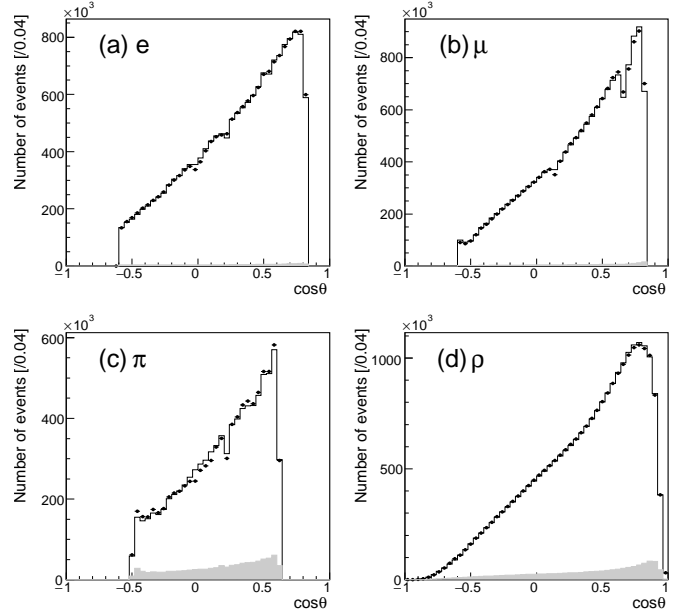


FIG. 2: The  $\cos\theta$  distributions of (a) electrons, (b) muons, (c) pions and (d)  $\rho$ 's for the samples obtained after all event selections in each mode. The points with error bars are the data, the histograms are the MC expectation, and the gray shaded histograms are the contribution from misidentification for each particle species.

the spin vector and the observables [17], experimentally the  $\tau$  direction cannot be uniquely determined because of the presence of two or more missing neutrinos. In the reactions where both  $\tau$  leptons decay semileptonically,  $e^+e^- \rightarrow \tau^+\tau^- \rightarrow A^+B^-\nu_\tau\bar{\nu}_\tau$  without initial-state radiation (ISR), the two possible solutions for the unit vector of the  $\tau^+$  flight direction,  $\hat{\mathbf{k}}_+$  and  $\hat{\mathbf{k}}_-$ , are given by

$$\hat{\mathbf{k}}_\pm = u\hat{\mathbf{p}}_A + v\hat{\mathbf{p}}_B \pm w \frac{\mathbf{p}_A \times \mathbf{p}_B}{|\mathbf{p}_A \times \mathbf{p}_B|}, \quad (10)$$

where  $\mathbf{p}_A$  ( $\mathbf{p}_B$ ) are the sum of three-momentum vectors in the decay products,  $A^+$  ( $B^-$ ), and the hats denote unit momenta. The parameters  $u$ ,  $v$ , and  $w$  are

$$u = \frac{\cos\theta_A + \hat{\mathbf{p}}_A \cdot \hat{\mathbf{p}}_B \cos\theta_B}{1 - (\hat{\mathbf{p}}_A \cdot \hat{\mathbf{p}}_B)^2}, \quad (11)$$

$$v = -\frac{\cos\theta_B + \hat{\mathbf{p}}_A \cdot \hat{\mathbf{p}}_B \cos\theta_A}{1 - (\hat{\mathbf{p}}_A \cdot \hat{\mathbf{p}}_B)^2}, \quad (12)$$

$$w = \sqrt{1 - u^2 - v^2 - 2uv(\hat{\mathbf{p}}_A \cdot \hat{\mathbf{p}}_B)}, \quad (13)$$

where  $\theta_A$  ( $\theta_B$ ) are the angles between the momenta of the decay product  $A^+$  ( $B^-$ ) and the  $\tau$  momentum:

$$\cos\theta_i = \frac{2E_\tau E_i - m_i^2 - m_\tau^2}{2|\mathbf{k}||\mathbf{p}_i|}, \quad (14)$$

where  $i = A$  or  $B$ . In this case, the  $\tau$  direction can be obtained with a twofold ambiguity. Experimentally this

TABLE I: Yield, purity, and dominant backgrounds for each selected mode. The purity and background are evaluated using MC simulation. The numbers in parentheses indicate the expected background rates in %.

Mode	Yield	Purity(%)	Background (%)
$e\mu$	6434268	95.8	$\gamma\gamma \rightarrow \mu\mu(2.5)$ , $\tau\tau \rightarrow e\pi(1.3)$
$e\pi$	2644971	85.7	$\tau\tau \rightarrow e\rho(6.5)$ , $e\mu(5.1)$ , $eK^*(1.3)$
$\mu\pi$	2503936	80.5	$\tau\tau \rightarrow \mu\rho(6.4)$ , $\mu\mu(4.9)$ , $\mu K^*(1.3)$ , $\gamma\gamma \rightarrow \mu\mu(3.1)$
$e\rho$	7218823	91.7	$\tau\tau \rightarrow e\pi\pi^0\pi^0(4.6)$ , $eK^*(1.7)$
$\mu\rho$	6203489	91.0	$\tau\tau \rightarrow \mu\pi\pi^0\pi^0(4.3)$ , $\mu K^*(1.6)$ , $\pi\rho(1.1)$
$\pi\rho$	2655696	77.0	$\tau\tau \rightarrow \rho\rho(6.7)$ , $\pi\pi\pi^0\pi^0(3.9)$ , $\mu\rho(5.1)$ , $\rho K^*(1.4)$ , $\pi K^*(1.4)$
$\rho\rho$	3277001	82.4	$\tau\tau \rightarrow \rho\pi\pi^0\pi^0(9.4)$ , $\rho K^*(3.1)$
$\pi\pi$	460288	71.9	$\tau\tau \rightarrow \pi\rho(11.3)$ , $\pi\mu(8.8)$ , $\pi K^*(2.5)$

ambiguity cannot be resolved. Therefore, we take an average of the two possible solutions in the calculation of the observables. In the case of leptonic  $\tau$  decays, one more ambiguity in the invariant mass of two neutrinos from the same  $\tau$ ,  $m_{\nu\nu}$ , arises as

$$\cos\theta_\ell = \frac{2E_\tau E_\ell - m_\ell^2 - m_\tau^2 + m_{\nu\nu}^2}{2|\mathbf{k}||\mathbf{p}_\ell|}. \quad (15)$$

We then take an average over multiple solutions using the MC method by varying  $m_{\nu\nu}$  uniformly within the possible kinematical range. For each event, we make 100 trials using a “hit-and-miss” approach while varying the effective mass  $m_{\nu\nu}$  randomly. With  $N_{\text{hit}}$  successful trials in which the  $\tau$  direction can be constructed kinematically, the average value of the observable is obtained for each event. In the case where both  $\tau$ 's decay leptonically, the  $m_{\nu\nu}$  is varied for each  $\tau$ . In the calculation, we require  $w$  in Eq. (13) be real and  $\cos\theta_j$  ( $j = A, B, \ell$ ) in Eqs. (14) and (15) be within the range  $[-1, 1]$ , therefore we removed the cases when the above requirements were not satisfied. In the analysis, we neglect the effect of ISR for the calculation of the observables, and include it as a systematic source. The distributions of observables for the obtained samples are shown in Fig. 3, along with those obtained from MC simulations with no EDM.

To obtain the EDM values from the observables, we must know the relation between the EDM and the observables shown in Eq. (6). In order to take into account the finite detector acceptance, the use of the most probable (rather than actual) spin direction, the ambiguity from the resolution, the unknown  $\tau$  direction, and missing neutrinos, the relation between the EDM and the mean value of the observables,  $\langle\mathcal{O}_{\text{Re/Im}}\rangle$ , is evaluated using MC simulation for various values of the EDM. By fitting the relation with a linear function in Eq. (6), as shown in Fig. 4, the coefficients  $a_{\text{Re/Im}}$  and the offsets  $b_{\text{Re/Im}}$  are obtained, which are plotted in Fig. 5. As seen from the values of the coefficients,  $a_{\text{Re/Im}}$ , the  $\pi\rho$  and  $\rho\rho$  modes have the highest sensitivities for  $\text{Re}(d_\tau)$  and  $\text{Im}(d_\tau)$ , because of high spin analyzing power for  $\pi$  and  $\rho$  modes. Nonzero offsets seen for the imaginary part,  $b_{\text{Im}}$ , are due to a forward-backward asymmetry in

the detector acceptance. The effects of the background are also taken into account in these coefficients. The coefficients are corrected by the purity and the coefficients obtained using the background samples.

We examine a number of possible systematic effects on the EDM measurements. The corresponding results are listed in Table II. Differences between the data and simulation result in systematic uncertainties. To check for an asymmetry in the tracking systems, we analyze  $e^+e^- \rightarrow \mu^+\mu^-$  events. We measure the difference of the polar and azimuthal angle of the tracks between  $\mu^+$  and  $\mu^-$ , and then found shifts from the back-to-back direction of  $-0.67$  mrad for the polar angle and  $-0.03$  mrad for the azimuthal angle. By applying an artificial rotation to one of the charged tracks, we obtain residual values of the observables and find the results to be less than 10% of the statistical uncertainties.

There are small data–MC differences in the  $\rho$  and  $\pi^0$  mass distributions. These can be caused by an imperfect momentum reconstruction resulting in a systematic offset of the observables. We check the effect of a momentum shift of the charged tracks by applying a momentum scaling factor of 1.0026, which is estimated from the peak position of the  $\rho$  mass distribution. We also check the effect of a  $\pi^0$  momentum shift by applying the same factor assuming that the  $\rho$  mass difference is due to  $\pi^0$  momentum shift.

In the  $\pi^0$  invariant mass distribution, we observe a difference of 0.3% in the mass resolution between data and MC samples. This is due to data–MC difference in the reconstructed photon energy. We check the effect by changing the photon energies according to the difference found in a  $D^{*0} \rightarrow D^0\gamma$  study. The change of the observables is obtained by conservatively varying the photon energy to  $E_\gamma \pm \sigma$  for both photons from  $\pi^0$ , however the change is smaller than the other uncertainties.

The detector response depends on the particle charge, especially for electrons and pions. However, we know that the MC simulation does not reproduce this difference exactly. We compare the ratios of the yield  $N(A^+B^-)/N(A^-B^+)$ , where  $A$  and  $B$  denote the final-state particles,  $e$ ,  $\mu$ ,  $\pi$ , and  $\rho$ , between the data and MC,

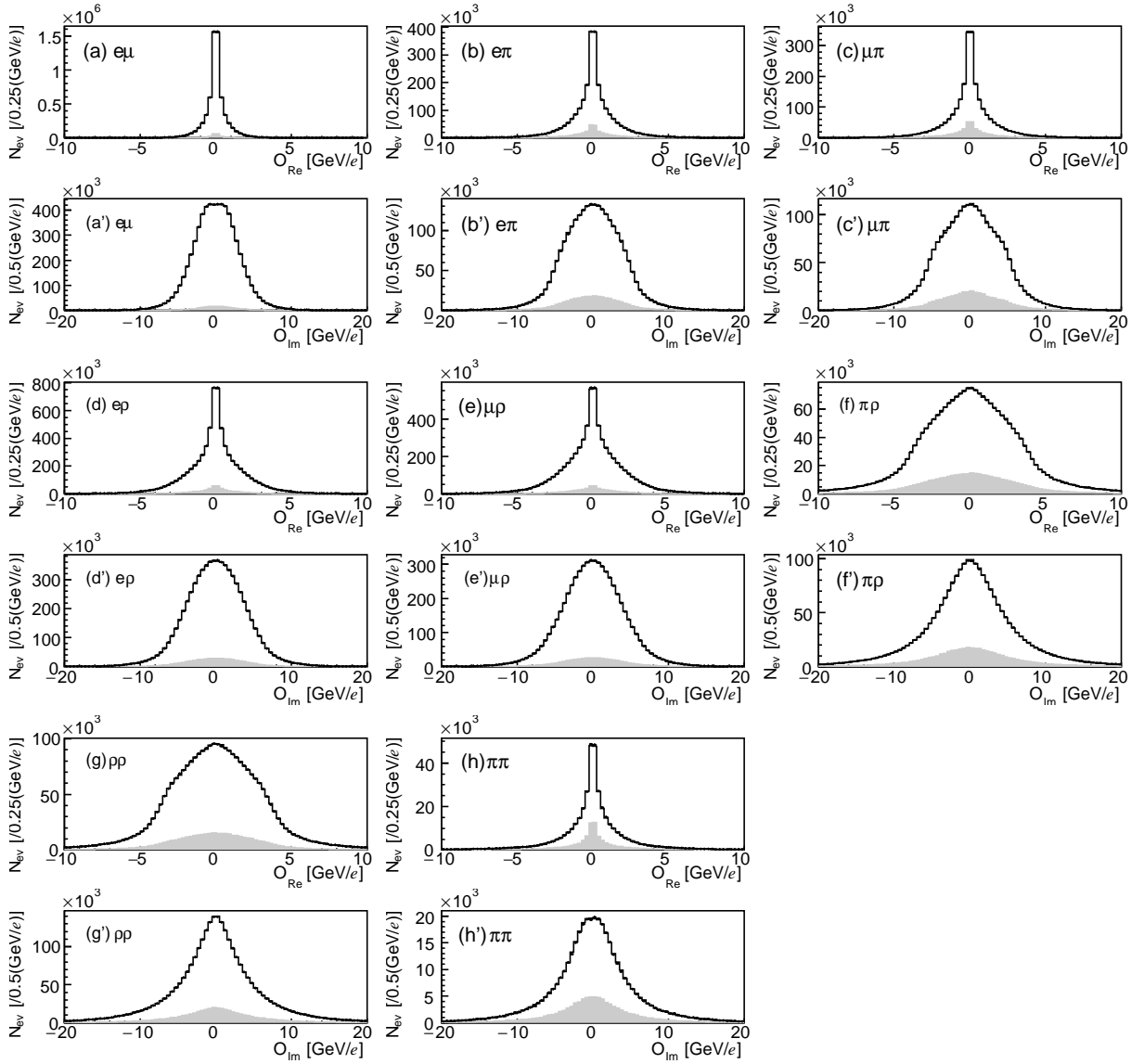


FIG. 3: Distributions of optimal observable for each mode. The upper (a)–(h) plots are  $\mathcal{O}_{\text{Re}}$  and the lower (a')–(h') plots are  $\mathcal{O}_{\text{Im}}$  for each mode. The points with error bars are the data and the histograms are the MC expectation with zero EDM. The gray shaded histograms are the background contribution estimated from simulation.

and find the difference in ratios to be about 1%. We apply the observed shift of the charge asymmetry on the yield to the efficiency and find a large systematic uncertainty on the offset of the imaginary part at the same level as the statistical uncertainty. (See the entries for  $\text{Im}(d_\tau)$  for the  $e\pi$  and  $\mu\pi$  modes in Table II.) The changes in other parameters are negligible.

We have also checked the polar angle dependence of the charge asymmetry. Although the data–MC consistency seems satisfactory, there are some differences. We also find a small difference between data and simulation in Figs. 1 and 2, where the momentum and polar angle distributions of the decay product are plotted. These differences are probably due to the reconstruction efficiency,

which causes a systematic offset. This effect is checked by re-weighting the MC samples with the weight functions constructed bin-by-bin from the data–MC ratio for the momentum and  $\cos\theta$  distributions, and independently of the charge. This is the largest source of systematic uncertainty for  $\text{Re}(d_\tau)$  in the high-sensitivity  $\pi\rho$  and  $\rho\rho$  modes.

In this analysis, the purity is obtained from simulation. Any difference in purity between the data and MC leads to a bias in the sensitivities and offsets. In order to take into account these possibilities, we include any difference of yields between the data and MC as a systematic uncertainty on the background level. The resulting systematic uncertainties are about 10% for the sensitivities and

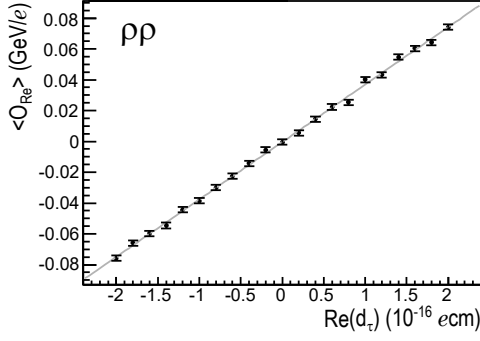


FIG. 4: Relation of  $\text{Re}(d_\tau)$  and  $\langle \mathcal{O}_{\text{Re}} \rangle$  for the  $\rho\rho$  mode obtained by the MC simulation. The line shows the fitted function. Other modes also show a similar linear dependence; the non-linearity is negligible for all modes.

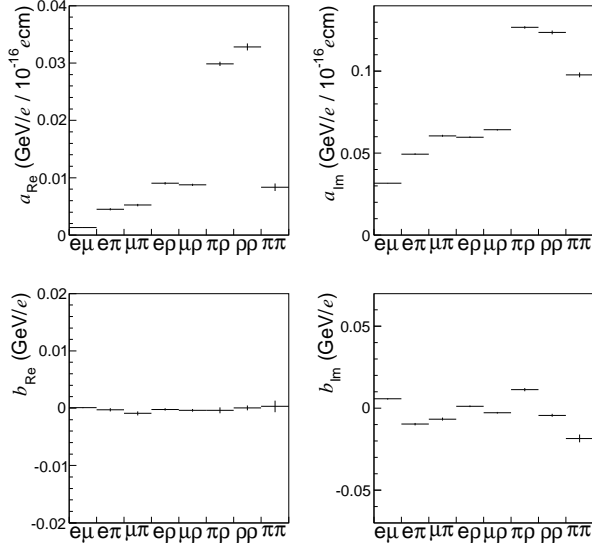


FIG. 5: EDM parameter sensitivity  $a_{\text{Re/Im}}$  (top) and offset  $b_{\text{Re/Im}}$  (bottom) for each mode. The uncertainties are due to the statistics of the MC samples.

about the same order of statistical uncertainties of the observables for the offsets.

In addition, we check the effect of ISR by introducing it into the calculation. We obtain the momenta of the ISR photons randomly from the KKMC generator, then, boost all momenta of the final-state particles into the  $\tau$ -pair rest frame assuming that the ISR is coming from the  $e^+e^-$  beam. We calculate the observables in this frame. We iterate this process 100 times using the same hit-and-miss approach as in the nominal analysis. For successful trials, we obtain the mean of the observables. The shifts and fluctuations with the ISR effect give estimates of the systematic effects of ignoring it.

We calculate the final EDM values using the 833 fb $^{-1}$  data sample, the results of which are listed in Table III for each mode. We obtain the mean values of the electric

dipole moment weighted by a quadrature sum of statistical and systematic uncertainties, for the real and imaginary parts,

$$\text{Re}(d_\tau) = (-0.62 \pm 0.63) \times 10^{-17} \text{ ecm}, \quad (16)$$

$$\text{Im}(d_\tau) = (-0.40 \pm 0.32) \times 10^{-17} \text{ ecm}. \quad (17)$$

The 95% confidence intervals become

$$-1.85 \times 10^{-17} < \text{Re}(d_\tau) < 0.61 \times 10^{-17} \text{ ecm}, \quad (18)$$

$$-1.03 \times 10^{-17} < \text{Im}(d_\tau) < 0.23 \times 10^{-17} \text{ ecm}. \quad (19)$$

Compared to the previous analysis [4], the obtained statistical uncertainties are reduced in proportion to the increase in the data size. The systematic uncertainties are improved because of the improved simulation, corrections and the larger statistics of the MC samples. The sensitivity for  $\text{Re}(d_\tau)$  and  $\text{Im}(d_\tau)$  has improved by about a factor of three. The systematic uncertainty from the detector modeling limits our result and needs to be controlled for future analysis.

## Appendix

The spin vectors used in the analysis are listed here.

For  $\tau \rightarrow \ell\nu_\ell\nu_\tau$ ,

$$\mathbf{S}_\pm = A \left( \pm m_\tau \mathbf{p}_{\ell^\pm} - \frac{c_\pm + E_{\ell^\pm} m_\tau}{k_0 + m_\tau} \mathbf{k} \right), \quad (20)$$

$$A = \frac{4c_\pm - m_\tau^2 - 3m_\ell^2}{3m_\tau^2 c_\pm - 4c_\pm^2 - 2m_\ell^2 m_\tau^2 + 3c_\pm m_\ell^2},$$

$$c_\pm = k_0 E_{\ell^\pm} \mp \mathbf{k} \cdot \mathbf{p}_{\ell^\pm},$$

where  $k_0$  is the energy of the  $\tau^\pm$ ,  $m_\tau$  is the  $\tau$  mass,  $\mathbf{k}$  is the three-momentum of the  $\tau^\pm$ ,  $\mathbf{p}_{\ell^\pm}$ ,  $E_{\ell^\pm}$  and  $m_\ell$  are the momentum, energy and mass of  $\ell^\pm$ , respectively.

For  $\tau \rightarrow \rho\nu_\tau \rightarrow \pi\pi^0\nu_\tau$ ,

$$\mathbf{S}_\pm = \mp A \left( \mp H_0^\pm \mathbf{k} + m_\tau \mathbf{H}^\pm + \frac{\mathbf{k}(\mathbf{k} \cdot \mathbf{H}^\pm)}{(k_0 + m_\tau)} \right), \quad (21)$$

$$A = \frac{1}{(k_\pm H^\pm) - m_\tau^2 (p_{\pi^\pm} - p_{\pi^0})^2},$$

$$(H^\pm)^\nu = 2(p_{\pi^\pm} - p_{\pi^0})^\nu (p_{\pi^\pm} - p_{\pi^0})^\mu (k_\pm)_\mu$$

$$+ (p_{\pi^\pm} + p_{\pi^0})^\nu (p_{\pi^\pm} - p_{\pi^0})^2,$$

where  $k_\pm = (k_0, \pm \mathbf{k})$ ,  $H^\pm = (H_0^\pm, \mathbf{H}^\pm)$ , and  $k_\pm H^\pm$  is the 4-vector product. Here,  $p_{\pi^\pm}$  and  $p_{\pi^0}$  are the four-momenta of the final state  $\pi^\pm$  and  $\pi^0$ .

We thank the KEKB group for the excellent operation of the accelerator; the KEK cryogenics group for the efficient operation of the solenoid; and the KEK computer group, and the Pacific Northwest National Laboratory (PNNL) Environmental Molecular Sciences Laboratory (EMSL) computing group for strong computing support; and the National Institute of Informatics, and Science Information Network 5 (SINET5) for valuable network support. We acknowledge support from the

TABLE II: Systematic uncertainties for  $\text{Re}(d_\tau)$  and  $\text{Im}(d_\tau)$  in units of  $10^{-17} e \text{ cm}$ .

$\text{Re}(d_\tau)$	$e\mu$	$e\pi$	$\mu\pi$	$e\rho$	$\mu\rho$	$\pi\rho$	$\rho\rho$	$\pi\pi$
Detector alignment	0.2	0.2	0.1	0.1	0.2	0.1	0.1	0.3
Momentum reconstruction	0.1	0.6	0.5	0.1	0.3	0.2	0.1	1.5
Charge asymmetry	0.0	0.0	0.1	0.0	0.0	0.0	0.0	0.0
Mismatch of distribution	3.2	4.8	3.8	0.9	2.2	0.9	0.9	3.6
Background variation	1.6	0.3	1.7	0.4	0.2	0.2	0.2	3.5
Radiative effects	0.7	0.5	0.6	0.2	0.2	0.0	0.0	0.1
Total	3.6	4.8	4.3	1.0	2.2	1.0	0.9	5.2
$\text{Im}(d_\tau)$	$e\mu$	$e\pi$	$\mu\pi$	$e\rho$	$\mu\rho$	$\pi\rho$	$\rho\rho$	$\pi\pi$
Detector alignment	0.0	0.0	0.0	0.0	0.1	0.0	0.0	0.0
Momentum reconstruction	0.2	0.5	0.4	0.0	0.1	0.1	0.1	0.1
Charge asymmetry	0.2	2.0	2.4	0.1	0.1	1.1	0.0	0.0
Mismatch of distribution	1.0	0.9	0.6	0.5	0.8	0.4	0.4	1.2
Background variation	1.4	0.0	0.7	0.3	0.1	0.1	0.1	0.1
Radiative effects	0.1	0.1	0.1	0.1	0.1	0.0	0.0	0.0
Total	1.8	2.2	2.6	0.6	0.8	1.2	0.4	1.2

TABLE III: Results on the  $\tau$  electric dipole moment obtained using  $833 \text{ fb}^{-1}$  of data. The first uncertainties are statistical and the second ones are systematic.

Mode	$\text{Re}(d_\tau)(10^{-17} \text{ ecm})$	$\text{Im}(d_\tau)(10^{-17} \text{ ecm})$
$e\mu$	$-3.2 \pm 2.5 \pm 3.6$	$0.6 \pm 0.4 \pm 1.8$
$e\pi$	$0.7 \pm 2.3 \pm 4.8$	$2.4 \pm 0.5 \pm 2.2$
$\mu\pi$	$1.0 \pm 2.2 \pm 4.3$	$2.4 \pm 0.5 \pm 2.6$
$e\rho$	$-1.2 \pm 0.8 \pm 1.0$	$-1.1 \pm 0.3 \pm 0.6$
$\mu\rho$	$0.7 \pm 1.0 \pm 2.2$	$-0.5 \pm 0.3 \pm 0.8$
$\pi\rho$	$-0.6 \pm 0.7 \pm 1.0$	$0.4 \pm 0.3 \pm 1.2$
$\rho\rho$	$-0.4 \pm 0.5 \pm 0.9$	$-0.3 \pm 0.3 \pm 0.4$
$\pi\pi$	$-2.2 \pm 4.3 \pm 5.2$	$-0.9 \pm 0.9 \pm 1.2$

Ministry of Education, Culture, Sports, Science, and Technology (MEXT) of Japan, the Japan Society for the Promotion of Science (JSPS) including in particular the Grant-in-Aid for Scientific Research (A) 19H00682, and the Tau-Lepton Physics Research Center of Nagoya University; the Australian Research Council including grants DP180102629, DP170102389, DP170102204, DP150103061, FT130100303; Austrian Federal Ministry of Education, Science and Research (FWF) and FWF Austrian Science Fund No. P 31361-N36; the National Natural Science Foundation of China under Contracts No. 11435013, No. 11475187, No. 11521505, No. 11575017, No. 11675166, No. 11705209; Key Research Program of Frontier Sciences, Chinese Academy of Sciences (CAS), Grant No. QYZDJ-SSW-SLH011; the CAS Center for Excellence in Particle Physics (CCEPP); the Shanghai Pujiang Program under Grant No. 18PJ1401000; the Shanghai Science and Technology Committee (STCSM) under Grant No. 19ZR1403000;

the Ministry of Education, Youth and Sports of the Czech Republic under Contract No. LTT17020; Horizon 2020 ERC Advanced Grant No. 884719 and ERC Starting Grant No. 947006 “InterLeptons” (European Union); the Carl Zeiss Foundation, the Deutsche Forschungsgemeinschaft, the Excellence Cluster Universe, and the VolkswagenStiftung; the Department of Atomic Energy (Project Identification No. RTI 4002) and the Department of Science and Technology of India; the Istituto Nazionale di Fisica Nucleare of Italy; National Research Foundation (NRF) of Korea Grant Nos. 2016R1D1A1B-01010135, 2016R1D1A1B02012900, 2018R1A2B3003643, 2018R1A6A1A06024970, 2018R1D1A1B07047294, 2019K1A3A7A09033840, 2019R1I1A3A01058933; Radiation Science Research Institute, Foreign Large-size Research Facility Application Supporting project, the Global Science Experimental Data Hub Center of the Korea Institute of Science and Technology Information and KREONET/GLORIAD; the Polish Ministry of Science and Higher Education and the National Science Center; the Ministry of Science and Higher Education of the Russian Federation, Agreement 14.W03.31.0026, and the HSE University Basic Research Program, Moscow; University of Tabuk research grants S-1440-0321, S-0256-1438, and S-0280-1439 (Saudi Arabia); the Slovenian Research Agency Grant Nos. J1-9124 and P1-0135; Ikerbasque, Basque Foundation for Science, Spain; the Swiss National Science Foundation; the Ministry of Education and the Ministry of Science and Technology of Taiwan; and the United States Department of Energy and the National Science Foundation.

- 
- [1] M. Kobayashi and T. Maskawa, *Prog. Theor. Phys.* **49**, 652 (1973).
- [2] M. J. Booth, hep-ph/9301293; U. Mahanta, *Phys. Rev. D* **54**, 3377 (1996).
- [3] T. Huang, W. Lum, and Z. Tao, *Phys. Rev. D* **55**, 1643 (1997); W. Bernreuther, A. Brandenburg, and P. Overmann, *Phys. Lett. B* **391** 413 (1997); *ibid.*, **412** 425 (1997).
- [4] K. Inami *et al.* (Belle Collaboration), *Phys. Lett. B* **551**, 16 (2003).
- [5] A. Abashian *et al.* (Belle Collaboration), *Nucl. Instrum. Methods Phys. Res., Sect. A* **479**, 117 (2002); also see Section 2 in J. Brodzicka *et al.*, *Prog. Theor. Exp. Phys.* **2012**, 04D001 (2012).
- [6] S. Kurokawa and E. Kikutani, *Nucl. Instrum. Methods Phys. Res., Sect. A* **499**, 1 (2003), and other papers included in the volume; T. Abe *et al.* *Prog. Theor. Exp. Phys.* **2013**, 03A001 (2013) and following articles up to 03A011.
- [7] W. Bernreuther, O. Nachtmann, and P. Overmann, *Phys. Rev. D* **48**, 78 (1993).
- [8] D. Atwood and A. Soni, *Phys. Rev. D* **45**, 2405 (1992).
- [9] S. Jadach, B.F.L. Ward, and Z. Wąs, *Comp. Phys. Commun.* **130**, 260 (2000); H. Burkhardt and B. Pietrzyk, *Phys. Rev. D* **72**, 057501 (2005).
- [10] R. Brun *et al.*, GEANT3.21, CERN Report No. DD/EE/84-1 (1987).
- [11] D. J. Lange, *Nucl. Instrum. Methods Phys. Res., Sect. A* **462**, 152 (2001).
- [12] F.A. Berends, P.H. Daverveldt, and R. Kleiss, *Comp. Phys. Commun.* **40**, 285 (1986).
- [13] K. Hanagaki *et al.*, *Nucl. Instrum. Methods Phys. Res., Sect. A* **485**, 490 (2002).
- [14] A. Abashian *et al.*, *Nucl. Instrum. Methods Phys. Res., Sect. A* **491**, 69 (2002).
- [15] Y. Ushiroda *et al.*, *Nucl. Instrum. Methods Phys. Res., Sect. A* **438**, 460 (1999).
- [16] Y. Tsai, *Phys. Rev. D* **4**, 2821 (1971); A. Posthaus and P. Overmann, *J. High Energy Phys.* **9802**, 001 (1998).
- [17] K. Ackerstaff *et al.* (OPAL Collaboration) *Z. Phys. C* **74**, 403 (1997).